Adhesion-related glycocalyx study: quantitative approach with imaging-spectrum in the energy filtering transmission electron microscope (EFTEM)

Mireille Soler[a], Sophie Desplat-Jego[a], Béatrice Vacher[c], Laurence Ponsonnet[c], Marc Fraterno[b], Pierre Bongrand[a], Jean-Michel Martin[c], Colette Foa[a,*]

[a] *Unité INSERM 387 'Adhésion Cellulaire', Hôpital Ste Marguerite, 13274 Marseille Cedex 9, France*
[b] *Service Commun de Microscopie Electronique, Faculté de Médecine, Bd Jean Moulin, 13005 Marseille, France*
[c] *Ecole Centrale de Lyon, Département de Technologie des Surfaces, URA CNRS 855, 36 Av. Guy de Collongue, 69131 Ecully, France*

Received 16 February 1998; revised version received 4 May 1998

Abstract Large polysaccharide molecules composing the glycocalyx have been shown to prevent cell adhesion. However, this process was not observed microscopically. Terbium labeling, combined with a new quantitative imaging method based on electron energy loss spectroscopy, allowed specific glycocalyx staining with excellent contrast. Image analysis enabled us to compare glycocalyx structure in free membrane areas and contacts between monocytic cells and bound erythrocytes. Apparent glycocalyx thickness, in contact areas, was half of the sum of glycocalyx thicknesses in free areas without label density increase. Ultrastructural immunogold localization of CD43 molecules, a major component of glycocalyx, was also demonstrated to be excluded from contact areas during adhesion. Thus, both approaches strongly suggest that some glycocalyx elements must exit from contact to allow binding of adhesion molecules.

Key words: Adhesion; Glycocalyx; Electron energy loss spectroscopy; Terbium; CD43; TPH-1 cell

1. Introduction

Adhesive interactions play an important role in many stages of the immune response, including antigen presentation [1], T-cell–B-cell interaction [2], T-cell mediated cytotoxicity [3] or phagocytosis of foreign particles [4].

Over the last few years, it has become apparent that the pericellular matrix might play an important regulatory role in adhesion. Indeed, it has long been reported that essentially all eukaryotic cells [5], including cells from the immune system [6], are coated with an electron light region several tens of nanometers thick. This size is markedly higher than the length of many adhesion molecules of the immune system [7]. These molecules correspond to two immunoglobulin domains, i.e. about 8 nm [8]. It is therefore easily conceivable that the presence of the cell coat during cell-to-cell approach might decrease adhesion efficiency [9].

Formation of extensive intercellular contact areas might require (i) compression of cell coat molecules, (ii) migration of repellers out of contact areas, and (iii) shedding of cell coat elements, and adhesion might be possible only in areas of the cell surface relatively depleted of glycocalyx elements.

In the present work, we tried to obtain some information on the above mechanisms by studying a model system. We chose to explore the interaction between immunoglobulin coated erythrocytes and human phagocytic THP-1 cells [10]; the advantages of this model are: (i) adhesion is biologically relevant since it is conducive to phagocytosis [11], (ii) red cells are fairly inert, which may facilitate data interpretation, and, at the same time (iii) they are surrounded by a fairly 'realistic' model of biological surfaces, and (iv) adhesion is mediated by Fc receptors and immunoglobulins of known structure.

In order to monitor the behavior of the cell coat during adhesion, we chose to obtain quantitative information on the structure of intercellular contact regions once the matrices were revealed by carbohydrate staining. Terbium, which selectively stains the glycoproteins and the proteoglycans [12], may be used to obtain quantitative information on the chemical composition of the glycocalyx when combined with an analysis technique such as electron energy loss spectroscopy (EELS), which allows quantitative determinations of the distribution of selected elements on electron microscopic images (ESI) [13–21]. In a previous work, we developed a method which makes it possible to perform quantitative imaging of terbium distribution with nanometer resolution. This method was called 'imaging-spectrum' [22,23]. We decided to obtain quantitative information on the size and density of the terbium stained glycocalyx molecules of free and intercellular contact regions.

We also tried to obtain some information on the above mechanism by studying the behavior of CD43 in the same model of adhesion. The CD43 molecule was chosen because this large [24] mucin-like glycoprotein [25] with numerous sialic acid moieties mediates an anti-adhesive effect. This molecule contributes to the glycocalyx and is involved in activation [26], adhesion [27] and inhibition of adhesion [28–30] in several immunological cells. Moreover, CD43 is altered in the Wiskott-Aldrich syndrome [31–33] and its role has not been fully elucidated in macrophages [34]. We localized CD43 at the ultrastructural level by immunogold and followed its behavior after adhesion. With the two approaches, we show the escape of some glycocalyx molecules from contact areas.

2. Materials and methods

2.1. Cells

The human monocytic (macrophage) THP-1 cell line [10] was cultured in RPMI 1640 medium (Biowhittaker, Verviers, Belgium), supplemented with 25 mM HEPES, 10% fetal calf serum (Biowhittaker), 2 mM L-glutamine (Biowhittaker), 50 U/ml penicillin (Biowhittaker), 50 μg/ml streptomycin (Biowhittaker) and $2\times10^{\times5}$ M β-mercapto-

*Corresponding author. Fax: (33) 4 91 75 73 28.
E-mail: foa@marseille.inserm.fr

PII S0014-5793(98)00570-5

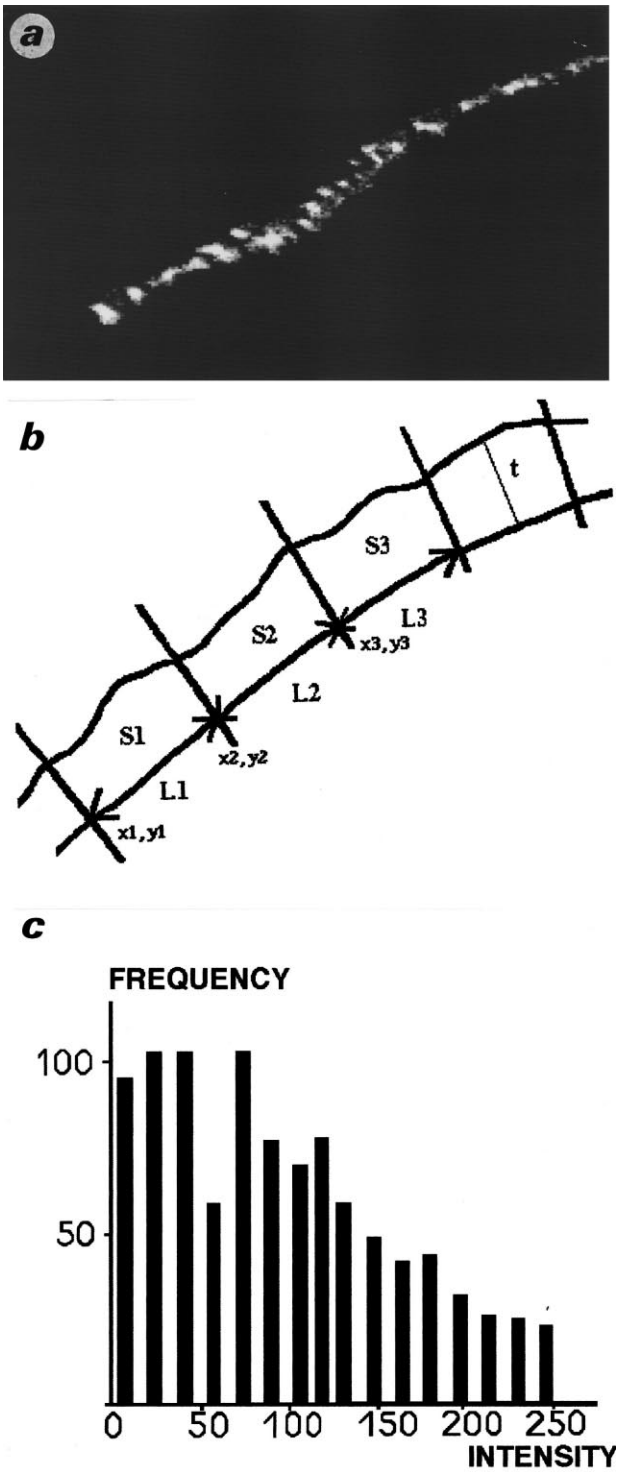

Fig. 1. a: An 'imaging-spectrum' (×20 000) of terbium stained glycocalyx treated with Adobe Photoshop software. b: Manual determinations of the boundaries delineate glycocalyx areas of about 0.5 μm long and give for each zone the surface in pixel (S) and the length (L) deduced from the coordinates of the ends of each zone and therefore make it possible to calculate the thickness (t) as the ratio S/L. c: Histogram of brightnesses of a delineated zone obtained with 255 grey level resolution.

ethanol (Sigma, St. Louis, MO USA). Cells were incubated at 37°C with 5% CO_2 and 100% humidity and subcultured 2–3 times a week. After each incubation period, cells were counted and viability was assessed by the trypan blue exclusion test. Sheep red blood cells (RBC) were purchased from Bio-Mérieux (Lyon, France) and used less than 1 month after delivery.

2.2. Adhesion tests

THP-1 cells were collected, washed three times in PBS and suspended at a concentration of 5×10^6 cells/ml in 200 μl PBS, pH 7.2. Sheep RBC were opsonized with anti-sheep RBC antibodies (1/50) (Sigma) at 4°C, washed three times in PBS and suspended at a concentration of 10^8 cells/ml. 100 μl of the suspended erythrocytes were allowed to adhere to THP-1 cells by centrifugation at $1200\times g$ for 20 s at 20°C in the presence of 0.03% sodium azide to avoid phagocytosis. Pellets were fixed in PBS containing 0.75% glutaraldehyde (Fluka, Buchs, Switzerland) and observed under the microscope. Adhesion was defined as the number of THP-1 cells binding at least two RBC. These conditions, determined by preliminary experiments, yielded about 60% adhesion. Non-opsonized RBC did not adhere to THP-1 cells in the same conditions.

2.3. Conventional electron microscopy

For conventional transmission electron microscopy (TEM), cells were fixed in 2.5% glutaraldehyde in 0.2 M cacodylate buffer, pH 7.2, rinsed twice and postfixed for 1 h in 1% osmium tetroxide in the same buffer. After dehydration in alcohols, cells were embedded in Araldite. Ultrathin sections were obtained with a Reichert Ultracut microtome and observed without any counterstaining in a Jeol 400C (Japan) electron microscope.

2.4. Glycocalyx staining

Terbium staining was performed according to Fehrenbach et al. [12]. Cells were fixed in 2.5% glutaraldehyde in 0.05 M cacodylate buffer containing 0.43% terbium chloride hexahydrate for 20 min at room temperature. After two rinses in the same buffer, cells were postfixed in 1% osmium tetroxide and processed as described above.

2.5. Electron spectroscopic imaging: imaging-spectrum EELS

The system is based on a Zeiss CEM902 (Oberkochen, Germany) microscope which is coupled to a Kontron IBAS image analysis system and linked to Visilog image analysis software running on a

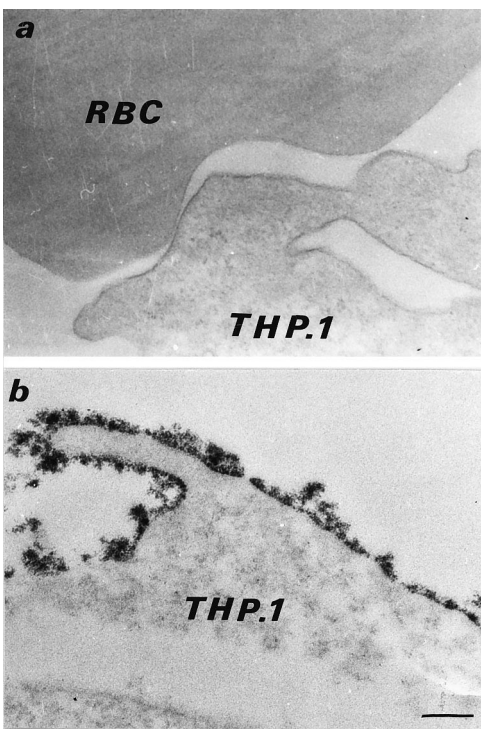

Fig. 2. TEM: a: after conventional processing, without counterstaining, the cell membrane of THP-1 cell is slightly delineated whereas RBC membrane and glycocalyx are not visible. b: After terbium staining, glycocalyx is strongly evidenced. Bar = 0.2 μm.

Hewlett-Packard workstation. A PC is added to the network for image archiving and rapid processing. The images are acquired via a DAGE SIT 66 camera which has a low detection level. Series of 48 images, 256×256 pixels, are recorded between two energy losses enclosing a given energy loss corresponding to the element to be detected with a given energy step between two images of the series (typically two series provide a sufficient energy loss range). Once the series is recorded it is possible to select, with a simple click of a mouse button, an area or a particular cluster of interest. The computation process reads each grey level for each selected pixel of each image and plots a curve, energy loss versus grey level, resulting in a corresponding partial EELS spectrum. The recording time depends on the energy of the edge of interest (the lower the energy loss, the lower the acquisition time) and varies from 60 to 300 s. The post-processing is of great importance because two major operations are performed on the recorded images: the spatial corrections and the elemental imaging calculations. Two spatial corrections must be made: the first is a shading correction required to take care of two phenomena: focalization of the electron beam and signal dispersion in the camera. The second correction concerns the drift of the specimen over long acquisition times. For the elemental calculation the imaging-spectrum method offers great potential for the choice of the images and the background calculation method (two or three image methods). Networking allows a direct dialogue between the microscope and the external environment. For terbium we used the $N_{4,5}$ edge located between 134 and 144 eV.

2.6. Image analysis of terbium 'imaging-spectrum'

Once stored on disks from the Zeiss CEM 902 electron microscope accessories, the 'imaging-spectra' (20 000× magnification), all obtained in the same conditions, were visualized (Fig. 1a) and analyzed with Adobe Photoshop software (MacIntosh Version 3.0). It allowed manual determinations of the boundaries. So it was possible to delineate glycocalyx areas of about 0.5 μm long (Fig. 1b). With the aid of Photoshop software, it was easy to determine for each zone the surface in pixel (S), the length (L) deduced from the coordinates of the ends of each zone and therefore to calculate the thickness (t) as the ratio S/L. The mean brightness of the delineated zones was also obtained with 255 grey level resolution (Fig. 1c). Five to 15 such zones were delineated for each area (free or bound) and the means calculated.

2.7. Immunoelectron microscopy

After adhesion tests, cell pellets were fixed during 1 h in 2% paraformaldehyde and 0.075% glutaraldehyde in PBS, pH 7.4, dehydrated in increasing concentrations of ethylic alcohol (70%, 90% and 100%), embedded in Unicryl (Biocell) and polymerized under UV illumination for 72 h. All steps were performed at 4°C. Ultrathin sections were

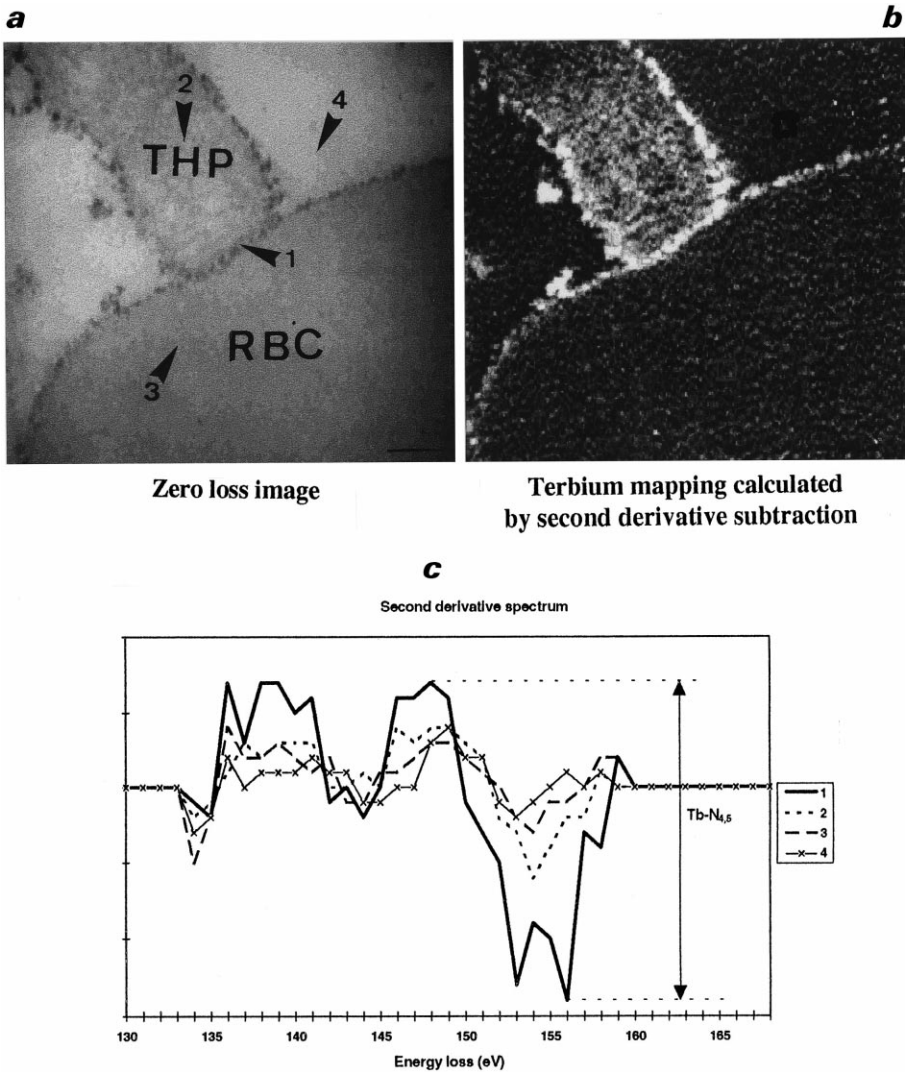

Fig. 3. Terbium stained glycocalyx of THP-1 and RBC cell contacts. a: Zero loss image. Terbium and osmium contribute to the electron dense staining. b: Terbium mapping with ESI. Brightness corresponds only to terbium and is correlated with its amount in the ultrathin section. (×15 000, bar = 0.5 μm); contrast is intense. c: Second derivative spectra show the presence of high amounts of terbium on the glycocalyx (1) of contact areas, and very low amounts in THP-1 and RBC cell cytoplasm (2 and 3) and none in araldite (4)

layered on nickel-copper grids and immunostained. Briefly, sections were exposed for 10 min to $ClNH_4$ (50 mM) in PBS pH 7.4, 20 min in PBS-SVF (10%), 60 min with monoclonal antibodies (anti-CD43: L60 (Becton Dickinson, San Jose, CA, USA), 1.25 μg/ml or isotypic control, IgG_1 (Immunotech, Marseille, France) 2.5 μg/ml). After five rinses of 10 min each in PBS-SVF, grids were incubated with 10 nm colloidal gold conjugated anti-mouse IgG (Biocell, Cardiff, UK) 1/30, rinsed successively in PBS-SVF, PBS and distilled water and observed with the electron microscope.

3. Results

3.1. Terbium stains glycocalyx with high specificity

With TEM, after conventional processing, without any counterstaining, cell membranes are slightly delineated but glycocalyces which are not electron dense are not visible on electron micrographs (Fig. 2a). After terbium staining [12] glycocalyces are strongly evidenced (Fig. 2b). With EELS, in our working conditions, the zero loss image demonstrated the presence of deposits mainly in the glycocalyx (Fig. 3a) and the contrast resulting mainly from the presence of terbium and osmium was rather good. To image terbium distribution, the selected area EELS spectra were derived in order to allow background subtraction and to increase the signal/noise ratio for the terbium $N_{4,5}$ edge located near 145 eV. Therefore, as shown in Fig. 3b, the contrast was maximal on terbium images. In particular, glycocalyx was very accurately delineated on THP-1 cells whereas araldite and cytoplasm of RBC were devoid of any deposit and appeared completely black. However, some brightness is observed in THP-1 cell cytoplasm.

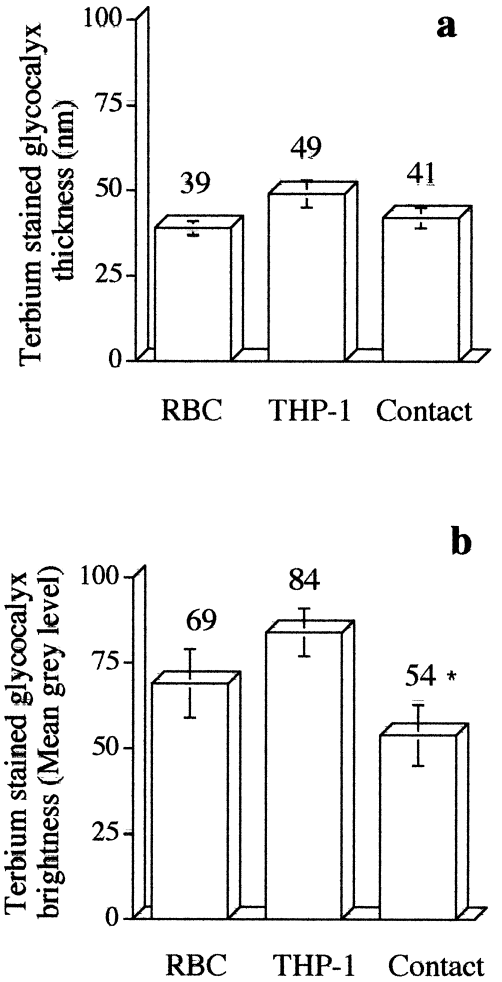

Fig. 4. a: Terbium stained glycocalyx thicknesses in free and bound areas of THP-1 and RBC cells. Mean of respectively 9, 11, and 7 zones of several micrometers. b: Terbium stained glycocalyx brightness (mean grey levels) in free and bound areas of THP-1 and RBC cells corresponding to the same zones. *Decrease of brightness in contact areas is significantly lower ($P < 0.025$) than in THP-1 cell free areas.

3.2. Terbium stains glycocalyx in contact areas between THP-1 and RBC cells

As seen in Fig. 3a, terbium stained glycocalyx in both free and contact areas between THP-1 and red blood cells. On zero loss images (Fig. 3a), glycocalyx was dark and cytoplasm remained pale, suggesting very low penetration of terbium into the cell. This was confirmed on images obtained at the $N_{4,5}$ terbium edge (Fig. 3b) where glycocalyx appeared very bright whereas RBC cytoplasm was rather black and THP-1 cell cytoplasm displayed very few deposits. Double derivative spectra clearly evidenced the presence of high amounts of terbium in the glycocalyx, its low amount in the cytoplasm and its absence in the araldite (Fig. 3c).

3.3. Terbium stained glycocalyx thickness in THP-1–RBC bound areas is approximately half of the sum of glycocalyx thicknesses in free areas

Morphometric analysis of glycocalyx in free areas showed that THP-1 cells and RBC did not display very different thicknesses (respectively 49.5 ± 4 nm and 39 ± 2 nm) which are not significantly different from the thicknesses measured in contact areas (41 ± 3 nm) (Fig. 4a).

3.4. Terbium stained glycocalyx density in THP-1–RBC bound areas is not increased compared with free areas

As described above, the brightness of terbium images obtained by ESI is correlated with the amount of glycocalyx stained molecules. Therefore it was of interest to compare the mean grey levels in free and bound cell membranes. Fig. 4b clearly shows there were no obvious differences in RBC coat brightness, either in free or in contact areas. Conversely, cell coat brightness in THP-1–RBC contacts was decreased compared to THP-1 glycocalyx brightness in free areas ($P < 0.025$).

3.5. Ultrastructural immunolocalization of CD43

On electron micrographs of immunostained Unicryl sections, CD43 was found irregularly distributed on the cell surface (Fig. 5a) and often accumulated on the microvilli of THP-1 cells. Gold particles were absent from RBC membranes, as expected, showing the specificity of the staining. After adhesion with RBC, gold particles were scarce or absent in contact areas; Fig. 5b is representative of the observations.

4. Discussion

The imaging-spectrum method [22,23] was used here to confirm the hypothesis that the pericellular matrix might contain microdomains with different behavior during adhesion: pericellular coat elements might be concentrated in some microdomains and rejected from others. We wanted to know if the intercellular adhesion could modulate the pericellular cell coat density.

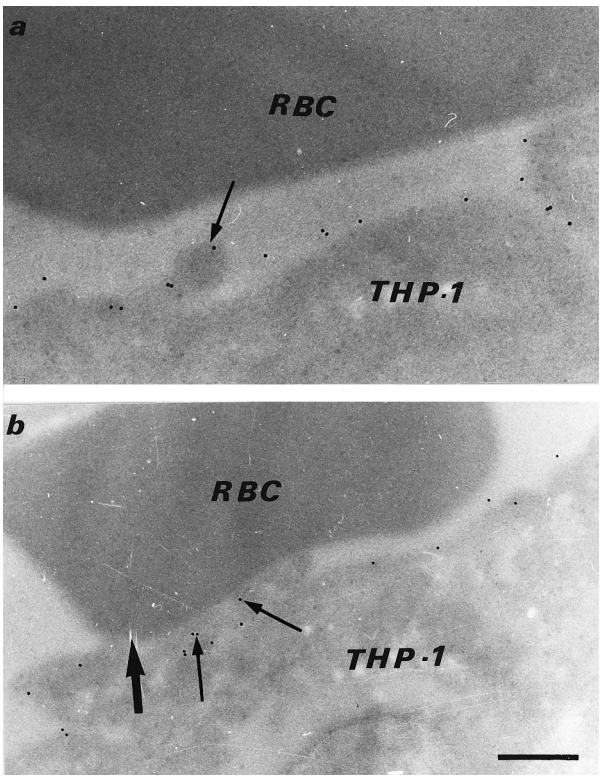

Fig. 5. Post-embedded immunogold localization of CD43 (with L60) on ultrathin Unicryl sections. Control experiments with irrelevant IgG1 yielded no labeling (data not shown). a: Gold particles (10 nm) are irregularly distributed in patches on the cell surface and preferentially accumulated on the microvilli (thin arrow). There is no labeling on RBC which do not display CD43 molecules. b: Gold particles are present on the microvilli and in the foldings of the membrane (thin arrow) but the contact areas are devoid of labeling (large arrow). Bar = 0.5 μm (×26 000).

Our results strongly support the use of terbium as an optimal reagent for staining the glycocalyx. Indeed, (i) terbium readily labeled the cell surface, in accordance with previous reports demonstrating that this cation bind mucopolysaccharides [35] as well as some phospholipids [36] and cation binding sites of proteins such as bovine serum albumin [37] or integrins [38]. (ii) In contrast with lanthanum ([39], and unpublished results), under our experimental conditions, terbium displays minimal penetration into the cytoplasm, thus yielding an excellent contrast. And (iii) specific detection of terbium distribution may be achieved with imaging-spectrum methodology.

According to Leapman and Andrews [40], EFTEM gave rise to problems of interpretation, i.e. it is sometimes difficult to be sure that the brightness of an image corresponds only to the presence of the element, particularly when high resolution is required. Our conditions of observation and acquisition of the images (described in detail in Section 2 and in our previous paper [23]) allowed us to assess that we obtained quantitative elemental maps of terbium and we present here a new quantitative approach of EFTEM applied to biology. However, some problems must be solved before our approach may be considered fully quantitative.

First, in our previous paper [39] we emphasized a difficult problem to overcome, which was the incidence of the plane of the section which was minimized, by the choice of the plane where the cell coat thickness was minimal. Stereological correction showed that the average apparent thickness of the intersection between the glycocalyx and the section plane of random orientation was twice the actual glycocalyx thickness as previously described [9].

Second, a crucial problem in quantitative determination of cell coat thickness and staining density is that insufficient spatial resolution of the apparatus might be responsible for an artefactual correlation between the two parameters: a decrease of staining density would result in an artefactual decrease of estimated cell coat thickness. It was difficult to definitely ascertain the glycocalyx thickness in our model and this was also the case in the literature as the proposed sizes differ greatly between various authors depending on the cell types and the mode of detection [7,8]. Moreover, glycocalyx is sometimes defined as the 10 nm thick zone above the plasma membrane whereas some authors (and ourselves) consider it is the thick stainable extracellular domain, including the mucin-like domain which extends 200–500 nm in extreme cases [41].

Third, we also have to keep in mind that this macromolecular organization could be altered because of the collapse of the cell coat with fixation and dehydration [42,43].

Fourth, terbium staining intensity in ESI resulted from the number of stained molecules in the ultrathin sections, the thickness of which was about 60 nm. If we assume that all ultrathin sections had the same thickness (which is only partially true as the variation could be 10 nm), we conclude that variations in glycocalyx grey levels resulted from variations in density of terbium stained molecules.

Despite these difficulties, our results strongly support the view that cell adhesion involved the exit of a proportion of glycocalyx elements from contact areas. Indeed, a part of the glycocalyx molecules had to be compressed after adhesion since the terbium thickness in bound areas was not higher than in free areas; second, a part of the cell coat molecules have probably migrated from contact areas since the terbium density in bound areas is not the sum of the densities in THP-1 cells and RBC free areas. Moreover, cell coat brightness in contact areas is lower than in free areas of THP-1 cells. Lee et al. [41] have proposed following an adaptation of De Gennes' model [44] that proteoglycans could exhibit two configurations: 'brush-like' and 'mushroom', depending on their density. It is then possible that cell coats modified their configuration in the contact areas. Moreover, we demonstrated the mobility of CD43 and its redistribution during adhesion.

Ultrastructural immunogold localization performed on post-embedded material is expected to give reliable results for pericellular labeling [45]. Immunogold is highly specific and labeling occurred on THP-1 cell surface but neither in the cytoplasm nor on RBC. The extent of labeling is not very high but it is known that labeling efficiency cannot be better in our conditions [45], which ensure good morphological preservation of contact areas. Labeling was absent from contact areas (clearly demonstrating the redistribution of CD43 after adhesion). A lack of access of the monoclonal antibodies to the antigenic site was not probable as gold particles were visible in the folds of the microvilli (Fig. 5b), the access to which did not seem easier than in contact areas. CD43 redistribution could not result from cross-linking of monoclonal antibodies as the localization of the molecule is performed on post-embedded sections. Similar results were obtained by immunofluorescence on living cells [46]. Such

migration of the molecule was also demonstrated in lymphoid cells where stimuli such as attachment to fibronectin or VCAM-1 induced a polarization at the cell uropod in the presence of CD43 monoclonal antibodis [47].

In conclusion, once EFTEM begins to be employed in biology [40], ESI will be rarely used as a quantitative method [48] and we propose it as a very sensitive method, convenient to detect variations of pericellular molecules during adhesion in agreement with the results of immunoelectron microscopy.

Acknowledgements: Supported by research grants from the Institut National de la Santé et de la Recherche Médicale, France.

References

[1] Springer, T.A., Dustin, M.L., Kishimoto, T.K. and Marlin, S.D. (1987) Annu. Rev. Immunol. 5, 223–252.
[2] Clark, E.A. and Lane, P.J.L. (1991) Annu. Rev. Immunol. 9, 97–127.
[3] Bongrand, P., Pierres, M. and Golstein, P. (1983) Eur. J. Immunol. 13, 424–429.
[4] Capo, C., Garrouste, F., Benoliel, A.M., Bongrand, P. and Depieds, R. (1981) Immunol. Commun. 10, 35–43.
[5] Benett, H.S. (1963) J. Histochem. Cytochem. 11, 14–23.
[6] Carr, I., Everson, G., Rankin, A. and Rutherford, J. (1970) Z. Zellforsch. Microsk. Anat. 105, 339–349.
[7] Springer, T.A. (1990) Nature 346, 425–433.
[8] Valentine, R.C. and Green, N.M. (1967) J. Mol. Biol. 27, 615–617.
[9] Foa, C., Soler, M., Benoliel, A.M. and Bongrand, P. (1996) J. Materials Sci. 7, 141–148.
[10] Tsuchiya, S., Yamabe, M., Yamaguchi, Y., Kobayashi, Y., Konno, T. and Tada, K. (1980) Int. J. Cancer 26, 171–176.
[11] Bouvier, G., Benoliel, A.M., Foa, C. and Bongrand, P. (1994) J. Leukocyte Biol. 55, 729–734.
[12] Fehrenbach, H., Schmield, A., Brasch, F. and Richter, J. (1994) J. Microsc. 174, 207–223.
[13] Ottensmeyer, F.P. and Andrew, J.W. (1980) J. Ultrastruct. Res. 72, 336–348.
[14] Leapman, R.D. (1986) Ann. NY Acad. Sci. 483, 326–338.
[15] Egerton, R.F. (1986) Electron Energy Loss Spectroscopy in the Electron Microscope, Plenum Press, New York.
[16] Leapman, R.D. and Ornberg, R.L. (1988) Ultramicroscopy 24, 251–268.
[17] Shuman, H., Chang, C.-F. and Somlyo, A.P. (1986) Ultramicroscopy 19, 121–134.
[18] Hunt, J.A. and Williams, D.B. (1991) Ultramicroscopy 38, 47–73.
[19] Reimer, L. (1991) Adv. Electron Phys. 81, 43–126.
[20] Reimer, L., Zedke, U., Moesch, J., Schulze-Hillert, S.T., Ross-Messemer, M., Probst, W. and Weimer, E. (1992) EEL Spectroscopy: Refererence Handhook of Standard Data for Identification and Interpretation of Electron Energy Loss Spectra and for Generation of Electron Spectra Imaging, Carl Zeiss Electron Optic Division, Oberkochen.
[21] Van Puymbroeck, J., Jacob, W. and Van Espen, P. (1992) J. Microsc. 166, 273–287.
[22] Lavergne, J.L., Martin, J.M. and Belin, M. (1992) Microsc. Microanal. Microstruct. 3, 517–528.
[23] Lavergne, J.L., Foa, C., Bongrand, P., Seux, D. and Martin, J.M. (1994) J. Microsc. 174, 195–206.
[24] Woollett, G.R., Williams, A.F. and Shotton, D.M. (1985) EMBO J. 11, 2827–2830.
[25] Cyster, J.G., Shotton, D.M. and Williams, A.F. (1991) EMBO J. 10, 893–902.
[26] Park, J.K., Rosenstein, Y.J., Remold-O'Donnell, E., Bierer, B.E., Rosen, F.S. and Burakoff, S.J. (1991) Nature 350, 706–709.
[27] Rosenstein, Y., Park, J., Hahn, W.C., Rosen, F.S. and Bierer, B.E. (1991) Nature 354, 233–235.
[28] Ardman, B., Sikorski, M. and Stauton, D.E. (1992) Proc. Natl. Acad. Sci. USA 89, 5001–5005.
[29] Manjunath, N., Johnson, R.S., Staunton, D.E., Pasqualini, R. and Ardman, B. (1993) J. Immunol. 151, 1528–1534.
[30] Manjunath, N., Correa, M., Ardman, M. and Ardman, B. (1995) Nature 377, 535–538.
[31] Remold-O'Donnell, E., Kenney, D.M., Parkman, R., Cairns, L., Savage, B. and Rosen, F.S. (1984) J. Exp. Med. 159, 1705–1723.
[32] Remold-O'Donnell, E., Zimmerman, C., Kenney, D. and Rosen, F.S. (1987) Blood 70, 104–109.
[33] Remold-O'Donnell, E., Rosen, F.S. and Kenney, D.M. (1996) Blood 87, 2621–2631.
[34] Nong, Y.H., Remold-O'Donnell, E., LeBien, T.W. and Remold, H. (1989) J. Exp. Med. 170, 259–267.
[35] Ohyashiki, T., Ohtsuka, T. and Ohri, T. (1985) Biochim. Biophys. Acta 817, 181–186.
[36] Petersheim, M., Halladay, H.N. and Blodniek, J. (1989) Biophys. J. 56, 551–557.
[37] Jin, Y., Li, W. and Wang, Q. (1991) Biochem. Biophys. Res. Commun. 177, 474–479.
[38] Cierniewski, C.S., Haas, T.A., Smith, J.W. and Plow, E.F. (1994) Biochemistry 33, 12238–12246.
[39] Foa, C., Soler, M., Fraterno, M., Passerel, M., Lavergne, J.L., Martin, J.M. and Bongrand, P. (1994) in: Studying Cell Adhesion (Bongrand, P., Claesson, P.M. and Curtis, A.S.G., Eds), pp. 219–224, Springer-Verlag, Berlin.
[40] Leapman, R.D. and Andrews, S.B. (1991) Microsc. Microanal. Microstruct. 2, 387–394.
[41] Lee, G.M., Zhang, F., Ishihara, A., McNeil, C.L. and Jacobson, K. (1993) J. Cell Biol. 120, 25–35.
[42] Clarris, B.J. and Fraser, J.R.E. (1968) Exp. Cell Res. 49, 181–193.
[43] Barber, P.M., Fletcher, J.M. and Newman, H.N. (1993) J. Struct. Biol. 110, 180–187.
[44] De Gennes, P.G. (1987) Adv. Colloid Interface Sci. 27, 189–209.
[45] Griffiths, G. and Hoppeler, H. (1986) J. Histochem. Cytochem. 34, 1389–1398.
[46] Soler, M., Merant, C., Servant, C., Fraterno, M., Allasia, C., Lissitzky, J.C., Bongrand, P. and Foa, C. (1997) J. Leukocytes 61, 609–618.
[47] Sanchez-Mateos, P., Campanero, M.R., del Pozo, M.A. and Sànchez-Madrid, F. (1995) Blood 86, 2228–2239.
[48] Beckers, A.L.D., Gelsema, E.S., de Bruijn, W.C., Cleton-Soeteman, M.I. and van Eijk, H.G. (1995) J. Microsc. 183, 78–88.